HOW2POWER TODAY
Your Power Design Newsletter

Exclusive Technology Feature

ISSUE: April 2020

The Engineer's Guide To EMI In DC-DC Converters (Part 12): Predicting The Differential-Mode Conducted Noise Spectrum

by Timothy Hegarty, Texas Instruments, Phoenix, Ariz.

The development of low-loss power semiconductors combined with higher switching frequencies[1] and enhanced control techniques is contributing to the miniaturization and improved efficiency of dc-dc regulator circuits. However, the high slew-rate voltages and currents during switching commutations may generate severe conducted and radiated interferences within the regulator itself (the electromagnetic interference (EMI) source) as well as nearby susceptible circuits (the EMI victims).

As a result, conducted emissions (CE) with higher amplitude are generated in the frequency measurement range of the electromagnetic compatibility (EMC) standards. An additional effort in the design of an EMI filter is thus essential to comply with the applicable standards. A careful dimensioning of the EMI filter enables high power density without penalizing system efficiency or cost.

Part 1 of this article series[2-12] reviewed the applicable EMI standards and the measurement approaches for conducted and radiated emissions. Part 2 then studied noise propagation and separation of differential-mode (DM) and common-mode (CM) emissions to understand the requisite attenuation from the EMI filter. Subsequently, parts 5 and 6 presented several EMI mitigation techniques for nonisolated regulator circuits, while parts 7 and 8 explored CM noise and its abatement in isolated designs. More recently, parts 10 and 11 considered the impact on stability and transient response when an input filter is connected to a regulated dc-dc converter.

In general, complying with EMC standards is an increasingly important task for switching power supplies, not because of excessive total spectral energy but more so the concentrated energy in specific narrow bands at the fundamental switching frequency and its harmonics. Custom-designed passive filtering at the input of a dc-dc regulator is the most common approach for mitigating EMI. To this end, part 12 now examines the modeling of DM noise, including the converter, passive EMI filter and measurement equipment.

Fig. 1a presents a conventional π-stage EMI filter for a dc-dc regulator. Fig. 1b shows the corresponding DM equivalent filter circuit as outlined in part 2. The design of such filters for use in power electronics applications is challenging, since the filters are terminated with varying impedances both at the noise source (the switching regulator) and the load (the power lines).

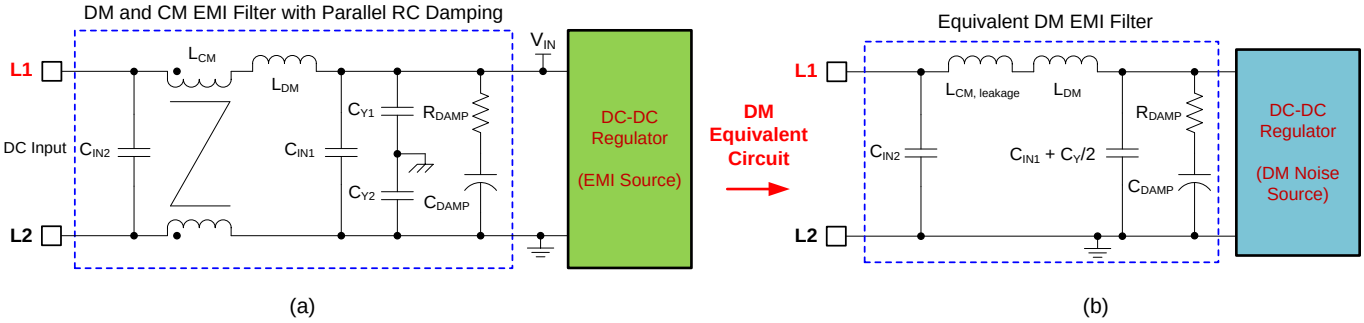

Fig. 1. An integrated DM and CM filter using passive components (a) and the equivalent circuit for DM noise currents (b). A parallel damping branch is represented by the series resistor and electrolytic capacitor.

This article takes into account the modeling of the converter and the measurement equipment, such as the line impedance stabilizing network (LISN) and the EMI test receiver (TR), in order to streamline and better predict the effectiveness of the DM filter design. The converter input current is modeled as a current source and its harmonic content is estimated by Fourier analysis.

Model Of The Passive EMI Filter

Occupying up to 50% of the total regulator solution size, a compact and efficient design for the EMI filter stage has become one of the most critical challenges in high-density dc-dc power converter design, particularly for automotive applications. The input filter of a dc-dc converter plays two important roles: one is to prevent EMI generated by the switching source from reaching the input power lines and affecting other equipment; the second is to protect the regulator and its load from input voltage disturbances,[13] thereby increasing system reliability and robustness.

Handoff of the line rejection task from the regulator control loop to the input filter attenuation characteristic ensures no break in the power-supply rejection performance over a wideband frequency range. With this in mind, the corner frequency of the input filter is generally placed one decade to one octave below the loop crossover frequency, depending on the rate of rolloff. As a simple example, Fig. 2 shows a synchronous buck converter with a switching frequency of 400 kHz. Setting the corner frequency of a single-stage LC filter at approximately 20 kHz, based on the values shown in Fig. 2, aligns with a loop crossover frequency of 60 kHz.

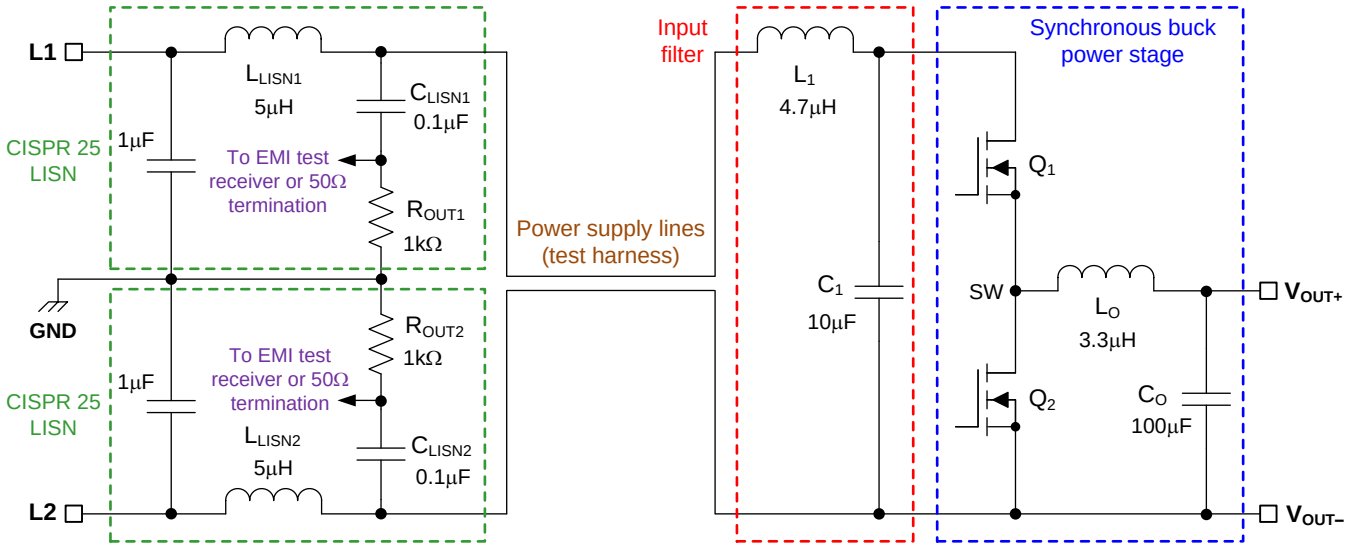

Fig. 2. Typical CE measurement setup for a synchronous buck converter with single-stage DM input filter and LISN circuit connected on each input line. The filter damping network is omitted here for simplification.

The input filter manages line transients by forward voltage attenuation and mitigates EMI by reverse current attenuation. Operating as a voltage filter from left to right in Fig. 2 with a transfer function expressed as the voltage ratio from input to output, the circuit also acts as a current filter from right to left to attenuate the ripple current and noise from the power stage. The transfer function characteristic is the same in either case, assuming low supply impedance (on the left) and high converter impedance (on the right).

Fig. 3 plots the forward voltage (or reverse current) attenuation of the filter stage in Fig. 2 with the component values for L_1 and C_1 as shown, assuming an inductor dc resistance (DCR) of 100 mΩ and a capacitor equivalent series resistance (ESR) of 10 mΩ. Fig. 3 indicates an attenuation of 15 dB at 60 kHz and 49 dB at 400 kHz.

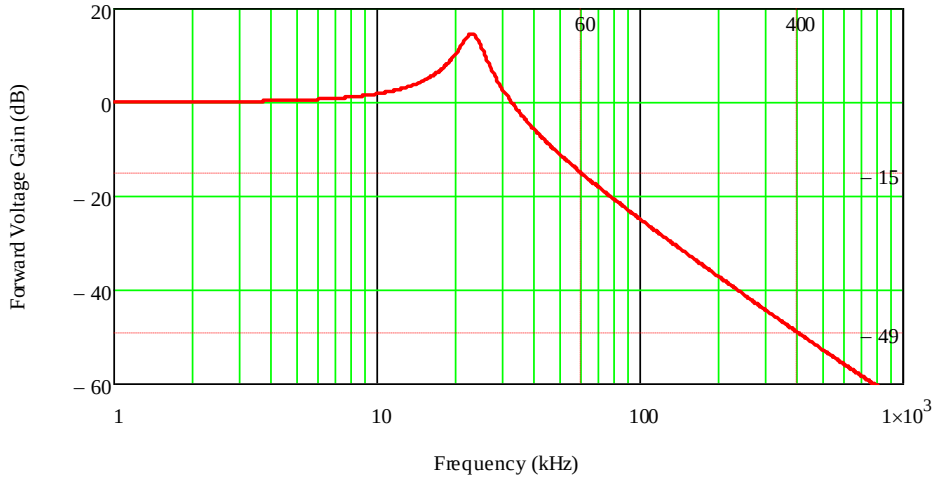

Fig. 3. Frequency response of the LC input filter (including inductor DCR and capacitor ESR first-order parasitics).

Model Of The LISN

Also included in Fig. 2 on each supply line L1 and L2 is a LISN measurement circuit, alternatively referred to as an artificial network, with component values as specified in Annex E of CISPR 25, a product standard for automotive. Connecting a LISN between the input supply and the equipment under test (EUT) provides a well-defined impedance and ensures reproducibility of the measurements. The test receiver then calculates the conducted emissions in units of decibel microvolts (dBμV) through the measurement of the voltage at the LISN measurement port, v_{TR}.

The values are similar for a LISN conforming to CISPR 16-1-1,[14] except the LISN inductance is 50 μH. The CISPR 16 and CISPR 25 LISNs are designed to operate up to 30 MHz and 108 MHz, respectively, based on the relevant frequency ranges for conducted emissions.

Fig. 4 shows a DM-equivalent circuit of the LISN in the mid- to high-frequency range (150 kHz to 108 MHz applies to CISPR 25 CE). An equivalent current source denoted as i_{dm} replaces the converter. The spectral composition of the converter input current waveform defines this current source, familiar examples being the trapezoidal input current waveform of a buck converter or the triangular ripple current waveform of a boost converter.

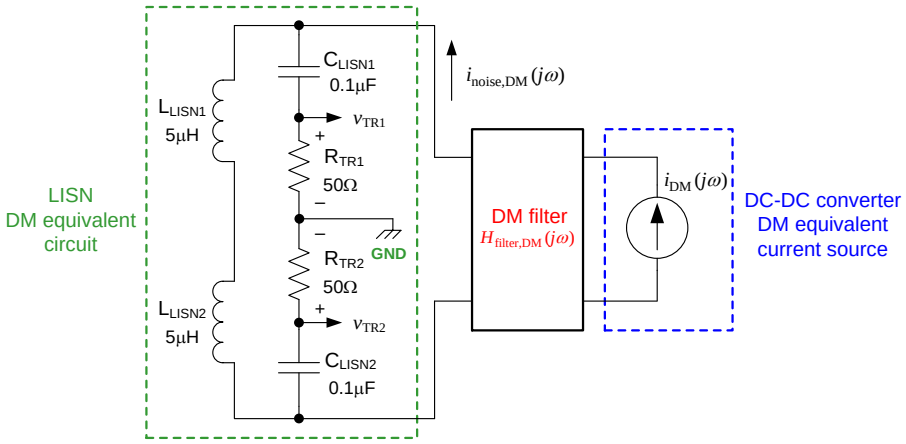

Fig. 4. A simplified high-frequency circuit model for determining DM conducted emissions through calculations or numerical simulation. A DM equivalent current source designated as i_{DM} models the converter.

The model is a good fit for circuit analysis, calculation of attenuation and estimation of impedances if the equivalent noise source is correctly modeled. Equation 1 gives the LISN transfer function from the filtered DM noise current to the LISN disturbance voltage (when connected to and measured by the TR):

$$G_{LISN}(s) = \frac{v_{TR1}(s)}{i_{noise,DM}(s)} = R_{TR}\frac{s^2 L_{LISN}C_{LISN}}{s^2 L_{LISN}C_{LISN} + sC_{LISN}R_{TR} + 1} \qquad (1)$$

Fig. 5 plots the LISN transfer function over frequency using the component values in Fig. 2. Also included is an equivalent plot for a CISPR 16 LISN. The impedance tolerance for both is ±20%.

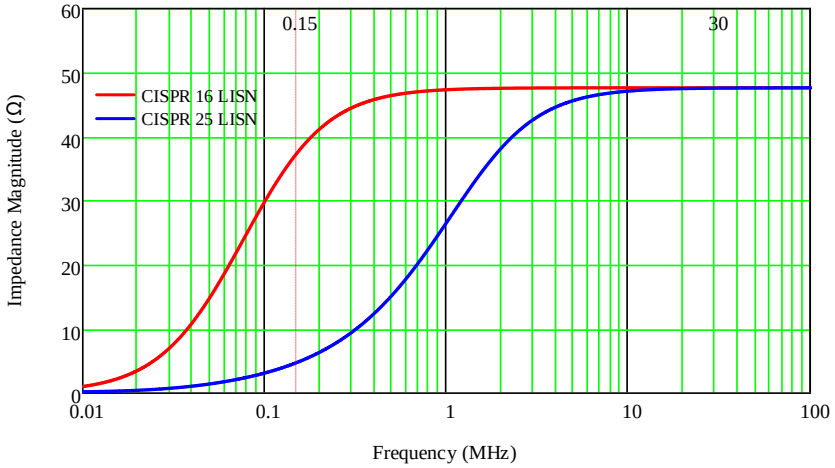

Fig. 5. Plot of LISN transfer function from noise current to measured voltage.

While both curves converge at high frequencies to 47.6 Ω, corresponding to the 50-Ω input resistance of the test receiver in parallel with the 1-kΩ discharge resistance of the LISN,[3] CISPR 25 specifies a lower LISN inductance of 5 μH based on the estimated inductance of an automotive harness, resulting in more current shunted from the measurement resistor at low frequencies. Surprisingly, the impedance of a CISPR 25 LISN is quite low below 1 MHz (4.8 Ω at 150 kHz)—much lower than the nominal 50 Ω presented by the test receiver.

Referring to Fig. 2 and using the frequency-domain transfer functions of the LISN and input filter, calculate the measured voltage spectrum $v_{TR}(j\omega)$ at the LISN output for a given spectrum of DM input current $i_{DM}(j\omega)$ with equation 2:

$$v_{TR}(j\omega) = i_{noise,DM}(j\omega)G_{LISN}(j\omega) = \left[i_{DM}(j\omega)H_{filter,DM}(j\omega)\right]G_{LISN}(j\omega) \qquad (2)$$

Assuming an ideal decoupling of the EUT from the input supply at high frequencies due to the LISN inductance, and a perfect coupling with the test receiver by the LISN capacitance, the high-frequency equivalent DM circuit of the LISN corresponds to $G_{LISN}(j\omega)$ = 47.6 Ω. The most simplified DM model of the dual LISN comprises the two measurement resistors in series, usually approximated as a total of 100 Ω.

As mentioned in part 2, when configured in a practical test setup, the LISN presents the total noise comprising DM and CM voltage components. A passive or active DM/CM noise separator circuit is then required to extract the DM noise signature. Treating the DM and CM components separately helps streamline the EMI filter design process. Part 13 will provide further context on this important topic.

DM Noise Model Of The Converter Input Current

The proper identification of the noise spectra followed by measurement with a test receiver[15-18] enables an early determination of filtering requirements and an efficient filter design workflow. Extending to high

frequencies is normally not required, since the largest components of the input filter have their size determined by the highest attenuation demand, which is typically at the lowest frequency to be filtered. Two main considerations apply here: higher frequencies are ideally well attenuated by the filter components, and the spectrum of a typical input current waveform decreases with frequency. Using Fourier analysis and sinusoidal basis functions, equation 3 represents a periodic function $S(t)$ by an infinite sum of sinusoidal components:

$$S(t) = c_0 + \sum_{n=1}^{\infty} 2\left|c_n\right| \cos\left(n\omega_s t + \angle c_n\right) \qquad (3)$$

where *n* is the harmonic order.

The Fourier series expansion coefficients for $n \geq 1$ are multiplied by a factor of two in equation 3 to account for a one-sided spectrum of positive frequencies. Equation 4 defines the coefficients:

$$c_n = \frac{1}{T_s}\int_{t_0}^{t_0+T_s} S(t) e^{-jn\omega_s t} dt \qquad (4)$$

As an example, consider the inductor current waveform of a boost converter as a periodic function with switching frequency f_s. Equation 5 provides the harmonic magnitudes of the triangular waveform based on Fourier analysis:

$$c_n(d,n) = \frac{\Delta i_{L\text{-}pp}}{n\pi}\left|\frac{\sin(n\pi d)}{n\pi d(1-d)}\right| = \frac{V_{out}}{L_b f_s \pi^2}\frac{\left|\sin(n\pi d)\right|}{n^2} \qquad (5)$$

where L_b and $\Delta i_{L\text{-}pp}$ are the boost inductance and ripple current amplitude, respectively; V_{out} is the output voltage; and *d* is the converter duty cycle.

The expressions for the Fourier coefficients of the boost inductor current are relatively simple if you neglect the parasitic current flow in the equivalent parallel capacitance of the inductor.

Fig. 6 shows the variation of the first four harmonic amplitudes as a function of duty cycle (due to a varying input voltage). While the first and second harmonics dominate on a percentage basis, the contribution from higher-order harmonics decreases rapidly. From equation 5, the spectral envelope rolls off with frequency at a rate of $1/n^2$, equivalent to -40 dB per decade. The fundamental frequency component requires the most attenuation and thus determines the size of the DM filter.

In a similar fashion, equation 6 gives the Fourier coefficients for the trapezoidal input current of a buck converter with duty cycle d. A second term set by finite rise and fall times, t_R and t_F, sets the duty factor d_r.

$$c_n(d,n) = I_{out} d\left|\frac{\sin(n\pi d)}{n\pi d}\right|\left|\frac{\sin(n\pi d_r)}{n\pi d_r}\right| \qquad (6)$$

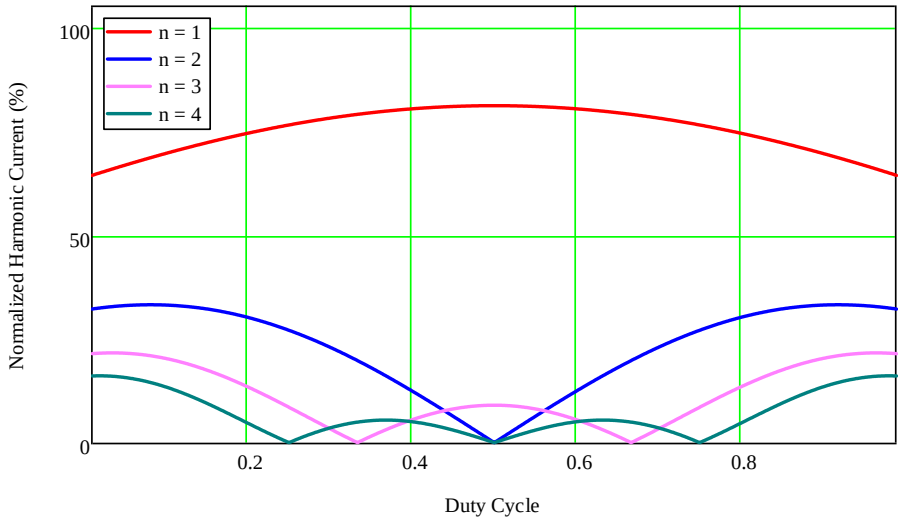

Fig. 6. Boost inductor current spectral harmonic content (normalized by the peak-to-peak ripple current amplitude) as a function of duty cycle.

Plotted in Fig. 7b, the harmonic envelope for the trapezoidal input current is a double sinc function with corner frequencies of f_1 and f_2, depending on the pulse width and rise/fall time of the time-domain waveform.[4] A ringing characteristic at the edges of the current waveform (arising from parasitic loop inductance or body-diode reverse recovery) can be represented by including the applicable frequency components from the measured current waveforms.

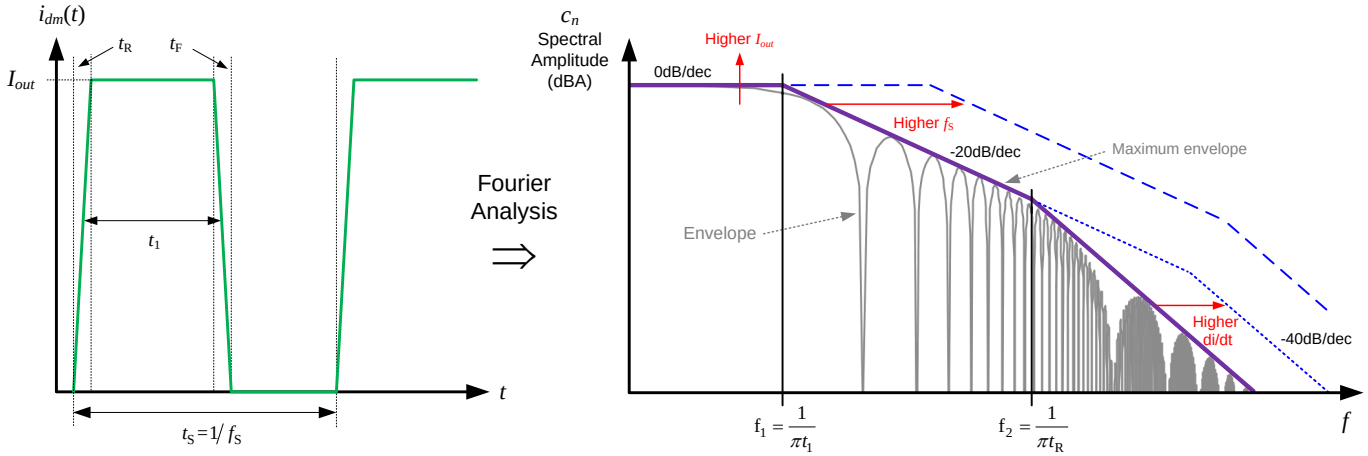

t_1 = pulse width (measured at half-maximum)
t_S = switching period; d = duty cycle = t_1/t_S

t_R = rise time; t_F = fall time of edge transition
d_r = rise/fall time duty factor = t_R/t_S or t_F/t_S

(a) (b)

Fig. 7. Buck converter input current waveform (a) and its spectral envelope impacted by duty cycle and rise/fall times (b).

Model Of The Test Receiver

The term "measurement receiver" generally refers to both EMI test receivers and spectrum analyzers.[19, 20] EMI test receivers function like spectrum analyzers (SAs) in accordance with the specifications stated in CISPR 16.

From this perspective, conventional SAs are used in EMC testing as long as they present features equivalent to a test receiver. However, the sensitivity and dynamic range of the SA are often not high enough, and the input stage is prone to overload. Test receivers present the bandwidth shapes, detector characteristics and dynamic range according to CISPR standards, along with high amplitude and frequency accuracies.

Time-domain mathematical modeling of the EMI receiver has recently been developed,[15] making it possible to define a procedure for EMI prediction. Fig. 8 shows a simplified block diagram of a test receiver based on the superheterodyne principle.

In a superheterodyne receiver, the input voltage is buffered and attenuated in the first stage and applied to a mixer, which multiplies the attenuated signal with the output of a tunable local oscillator. The output of the mixer is the input signal shifted by the output frequency of the local oscillator, enabling selection of the part of the input spectrum that is mapped to the center frequency of the intermediate frequency (IF) filter by tuning the frequency of the local oscillator.

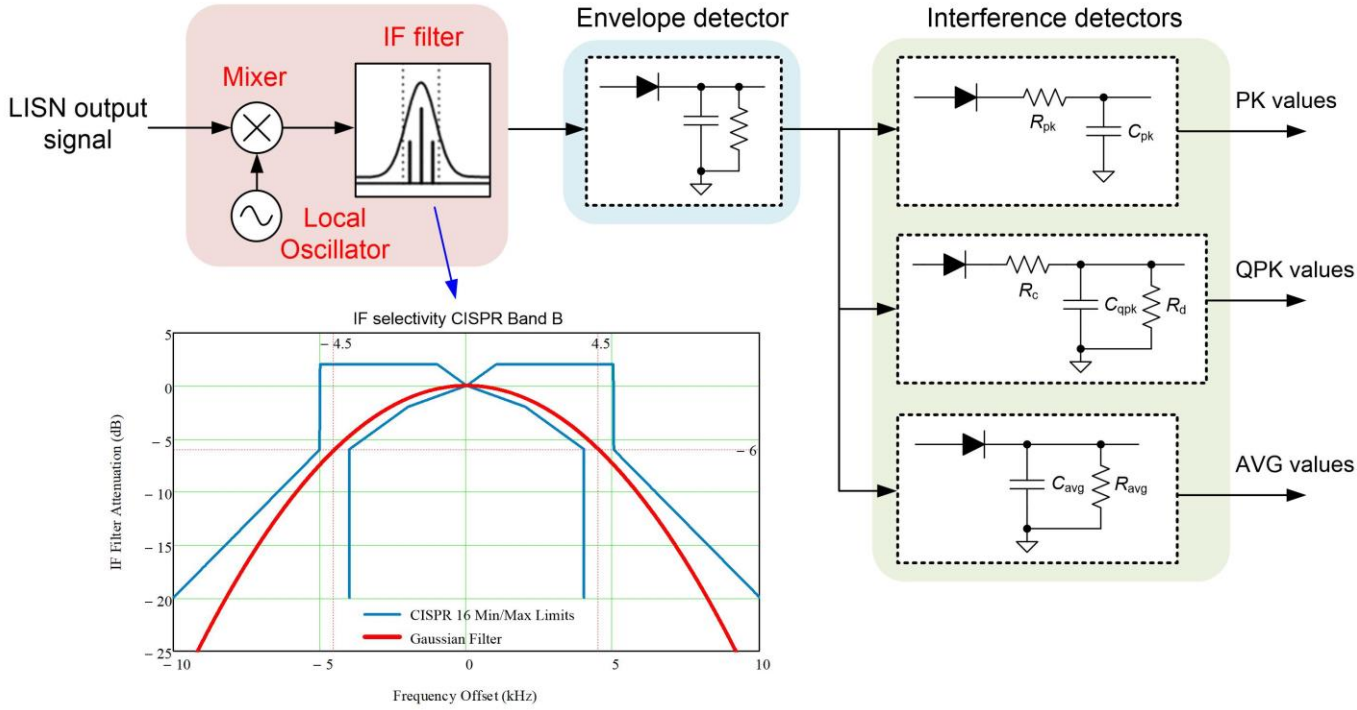

Fig. 8. Simplified heterodyne measurement and detection model of the test receiver. Dependent on the oscillator frequency, the mixer shifts the frequency of interest to an IF where the measurements are made, employing a fixed-frequency band-pass filter according to CISPR 16.

Equation 7 expresses the amplitude gain of the equivalent IF filter based on near-Gaussian filter theory:

$$\left|G_{\mathrm{IF}}\left(f, f_{\mathrm{IF}}\right)\right| = e^{-\left[\frac{(f-f_{\mathrm{IF}})\sqrt{\ln 2}}{\mathrm{f_{RBW}}/2}\right]^2} = \begin{cases} 0\,\mathrm{dB} \;\text{ at }\; f = f_{\mathrm{IF}} \\ -6\,\mathrm{dB} \;\text{ at }\; f = f_{\mathrm{IF}} \pm f_{\mathrm{RBW}}/2 \end{cases} \quad (7)$$

where f_{IF} is the center frequency of the equivalent IF filter.

The specified resolution bandwidth (RBW) of the IF filter is 9 kHz and 120 kHz in band B (150 kHz to 30 MHz) and in band C (30 MHz to 300 MHz), respectively. After the envelope detector stage shown in Fig. 8, several detector types are used for EMI measurement: peak (PK), quasi-peak (QPK) and average (AVG).

Equation 8 gives the expressions to calculate the detector output voltage by applying digital sampling to obtain the envelope detector values in one period, as shown in Fig. 9a. Given *N* evenly sampled data points in one period, as shown in Fig. 9a, the results for V_{peak} and V_{avg} of the envelope correspond to the maximum and averaged values of these sampled data points' V_i, respectively. Applying charge balance on the detector capacitor, as depicted in Fig. 9b, enables calculation of $V_{quasi\text{-}peak}$.

$$V_{peak} = \max\left(V_i\right)$$

$$\frac{\sum_{i=1}^{Q}\left(V_i - V_{quasi\text{-}peak}\right)}{R_c} = \frac{V_{quasi\text{-}peak}\,N}{R_d} \qquad (8)$$

$$V_{avg} = \frac{\sum_{i=1}^{N} V_i}{N}$$

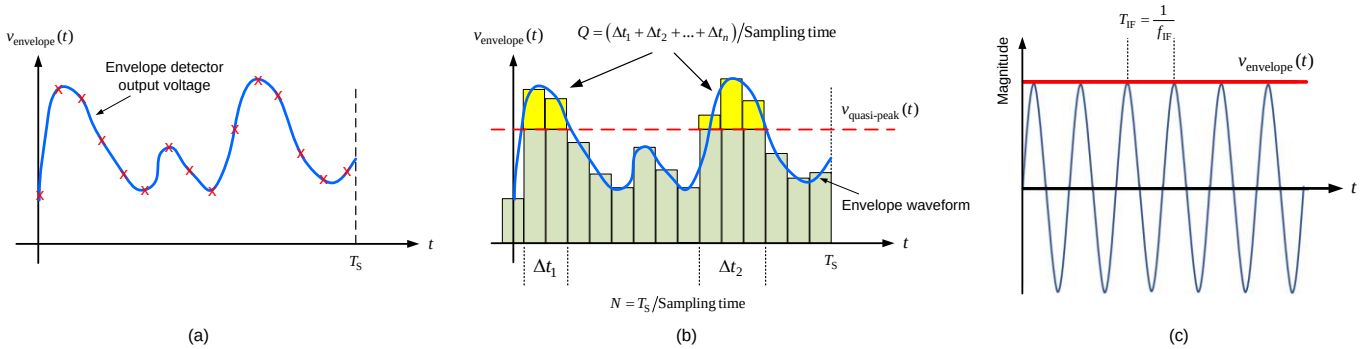

Fig. 9. Generalized envelope detector output voltage with N sampling points (a), quasi-peak detector capacitor charge balance (b), and envelope detector voltage with a fixed-frequency harmonic in the RBW (c).

In general, $V_{peak} \geq V_{quasi\text{-}peak} \geq V_{avg}$, with equality applying when the output voltage of the envelope detector has solely a dc component, as shown in Fig. 9c (for example, a fixed-frequency converter where the input signal is formed by a single harmonic component inside the RBW band pass). The final stage of the test receiver is a video filter characterized by a time constant of 160 ms, which removes the ripple from the detector output. Fig. 10 presents the flowchart for EMI noise prediction.[15]

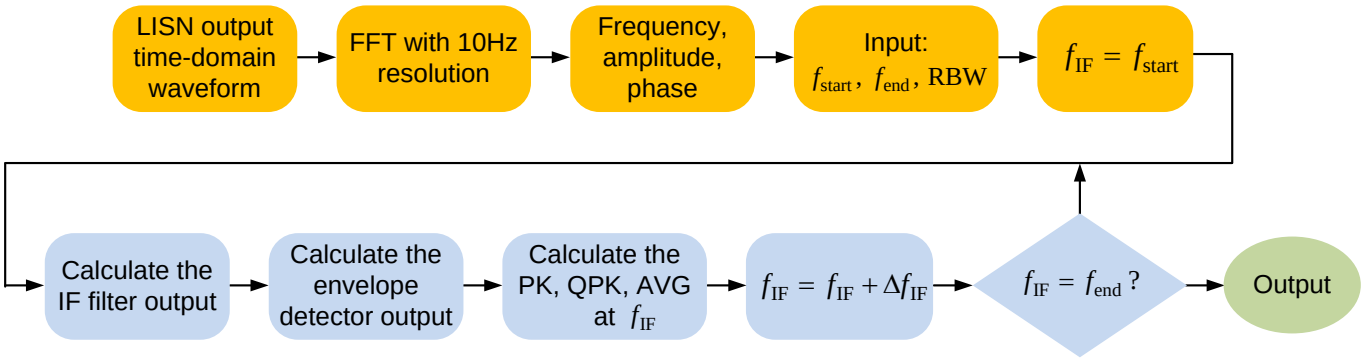

Fig. 10. Flowchart of EMI noise spectrum prediction algorithm.

Summary

This article provides an overview of how to predict the DM conducted noise spectrum, in particular at the frequency that dictates the DM filter design corresponding to the lowest-order switching harmonic above 150 kHz. This can save time and cost, as well as facilitate investigation of different noise-reduction methods. Fourier analysis of the input current waveform enables examination of a converter's DM noise spectrum. The next installment, part 13, will discuss DM filter design, leveraging the concepts outlined here to streamline the design process.

References

1. "A survey of EMI research in power electronics systems with wide-bandgap semiconductor devices" by Boyi Zhang and Shuo Wang, *IEEE Journal of Emerging and Selected Topics in Power Electronics*, Vol. 8, No. 1, March 2020, pp. 626-643.

2. "The Engineer's Guide To EMI In DC-DC Converters (Part 1): Standards Requirements And Measurement Techniques" by Timothy Hegarty, How2Power Today, December 2017 issue.

3. "The Engineer's Guide To EMI In DC-DC Converters (Part 2): Noise Propagation and Filtering" by Timothy Hegarty, How2Power Today, January 2018 issue.

4. "The Engineer's Guide To EMI In DC-DC Converters (Part 3): Understanding Power Stage Parasitics" by Timothy Hegarty, How2Power Today, March 2018 issue.

5. "The Engineer's Guide To EMI In DC-DC Converters (Part 4): Radiated Emissions" by Timothy Hegarty, How2Power Today, April 2018 issue.

6. "The Engineer's Guide To EMI In DC-DC Converters (Part 5): Mitigation Techniques Using Integrated FET Designs" by Timothy Hegarty, How2Power Today, June 2018 issue.

7. "The Engineer's Guide To EMI In DC-DC Converters (Part 6): Mitigation Techniques Using Discrete FET Designs" by Timothy Hegarty, How2Power Today, September 2018 issue.

8. "The Engineer's Guide To EMI In DC-DC Converters (Part 7): Common-Mode Noise Of A Flyback" by Timothy Hegarty, How2Power Today, December 2018 issue.

9. "The Engineer's Guide To EMI In DC-DC Converters (Part 8): Mitigation Techniques For Isolated Designs" by Timothy Hegarty, How2Power Today, February 2019 issue.

10. "The Engineer's Guide To EMI In DC-DC Converters (Part 9): Spread-Spectrum Modulation" by Timothy Hegarty, How2Power Today, August 2019 issue.

11. "The Engineer's Guide To EMI In DC-DC Converters (Part 10): Input Filter Impact On Stability" by Timothy Hegarty, How2Power Today, November 2019 issue.

12. "The Engineer's Guide To EMI In DC-DC Converters (Part 11): Input Filter Impact On Dynamic Performance," by Timothy Hegarty, How2Power Today, January 2020 issue.

13. "Front End Power Supply Reference Design with Cold Crank Operation, Transient Protection, EMI Filter," TI reference design TIDA-00699, November 2015.

14. "Specification for radio disturbance and immunity measuring apparatus and methods - Part 1-1: Radio disturbance and immunity measuring apparatus - Measuring apparatus," CISPR 16-1-1:2019, IEC 2019.

15. "Prediction and Analysis of EMI Spectrum Based on the Operating Principle of EMC Spectrum Analyzers" by Le Yang et al., *IEEE Transactions on Power Electronics*, Vol. 35, No. 1, January 2020, pp. 263-275.

16. "The Worst Conducted EMI Spectrum of Critical Conduction Mode Boost PFC Converter" by Qing Ji et al., *IEEE Transactions on Power Electronics*, Vol. 30, No. 3, March 2015, pp. 1230-1241.

17. "EMI-receiver simulation model with quasi-peak detector" by Timucin Karaca et al, *IEEE International Symposium on Electromagnetic Compatibility (EMC)*, Dresden, 2015, pp. 891-896.

18. "DM EMI Noise Prediction for Constant On-Time, Critical Mode Power Factor Correction Converters" by Zijian Wang et al., *IEEE Transactions on Power Electronics*, Vol. 27, No. 7, July 2012, pp. 3150-3157.

19. "Agilent Spectrum Analysis Basics," Application Note 150, Keysight Technologies (previously Agilent), 2004.

20. "Measuring with Modern Spectrum Analyzers," Educational Note, Rohde & Schwarz, February 2013.

About The Author

Timothy Hegarty is an applications engineer for the Buck Switching Regulators business unit at Texas Instruments. With over 22 years of power management engineering experience, he has written numerous conference papers, articles, seminars, white papers, application notes and blogs.

Tim's current focus is on enabling technologies for high-frequency, low-EMI, isolated and nonisolated regulators with wide input voltage range, targeting industrial, communications and automotive applications in particular. He is a senior member of the IEEE and a member of the IEEE Power Electronics, Industrial Applications and EMC Societies.

For more information on EMI, see How2Power's Power Supply EMI Anthology. Also see the How2Power's Design Guide, locate the Design Area category and select "EMI and EMC".